Spatio-Temporal analysis of the Volcanic Eruption Zone using SAR Interferometric Technique

Satwik Bhattacharya[1*], Shashi Kumar[1]

[1*]Photogrammetry and Remote Sensing Department, Indian Institute of Remote Sensing, India – geosatwik@gmail.com
[1]Photogrammetry and Remote Sensing Department, Indian Institute of Remote Sensing, India – shashi@iirs.gov.in

Keywords: Land deformation, volcanic eruption, InSAR, SBAS, PyGMTSAR.

Abstract

The phenomena of eruption induced land deformation are insightful for the understanding of the associated spatio-temporal processes. This study focusses on the same phenomena which was induces due to the Wolf Volcano's effusive type eruption that took place on the year 2022. The work has been conducted using the Small Baseline Subset (SBAS), a time-series Interferometric Synthetic Aperture Radar (InSAR) technique. The SBAS, a coherence-based approach comes in very handy for the study of a natural and uninhabited regions like the Wolf Volcano of the Galapagos Archipelago. The processing of the radar images was implemented using a python library specifically designed for SAR processing in Google Collab. The study concludes the displacement pattern intensified through the south-eastern flank of the volcano, showing a consistent uplift of up to ~50 mm, spatially aligned with the lava flow paths as lava effused southwards and a highlighted substantial subsidence ~60 mm in the line of sight direction of the satellite within the central caldera, likely due to post-eruptive deflation as magma evacuated from the shallow reservoir. The results were validated solely through comparison with other remote sensing studies. This is primarily due to the remote and protected status of Wolf Volcano, which restricts fieldwork. This study is necessary for the understanding of such regions which are protected and uninhabited but also have a dynamic geomorphic system.

1. Introduction

Volcanic eruptions are among the most dramatic and dynamic geological phenomena on Earth. These events are typically accompanied by pronounced geophysical and geochemical changes, including land deformation, gas emissions, seismic activity, and lava effusion. Monitoring these processes is critical for understanding volcanic dynamics, forecasting eruptions, and mitigating associated hazards to populations, infrastructure, and ecosystems (Kuraoka et al., 2018).

Wolf Volcano, the northernmost and highest volcano of Isabela Island in the Galápagos Archipelago, erupted on 7 January 2022 after nearly seven years of quiescence and approximately six years of inflation following its 2015 eruption (Xu et al., 2023). The 2022 eruption began along an ~8 km-long fissure on the south eastern flank, generating lava flows that travelled ~15 km and covered ~7–30 km² before halting 150–200 m from the coastline (Venzke, 2024). InSAR analyses of this eruption have revealed evidence of precursory inflation, co-eruptive deflation, and flank deformation (Xu et al., 2023). A recent study, *The 2022 Eruption of Wolf Volcano, Galápagos* (AGU Geophysical Research Letters), highlighted the onset of the shallow flank eruption after six years of inflation, underscoring the effectiveness of InSAR for monitoring volcanic processes (Xu et al., 2023).

Among remote sensing techniques, Synthetic Aperture Radar Interferometry (InSAR) has become a cornerstone for volcano monitoring. InSAR provides millimetre- to centimetre-level precision across large areas, detecting subtle surface displacements linked to subsurface magmatic activity, faulting, and crustal adjustments. Its weather-independent and all-day imaging capabilities make it particularly effective for remote volcanoes, where optical observations and ground surveys are limited (Lu et al., 2007).

Volcanic islands, especially those in isolated oceanic settings like the Galápagos, hold significant geomorphological and ecological interest. These islands experience frequent and rapid vertical displacements driven by hotspot volcanism, making them ideal natural laboratories for studying volcanic processes and island landscape evolution (Chadwick et al., 2006). At the same time, their ecological sensitivity and the presence of growing tourism-related infrastructure highlight the importance of hazard monitoring.

However, in situ monitoring methods such as GPS networks, tilt meters, and field surveys are often logistically and economically constrained in such remote and rugged terrains. Wolf Volcano, in particular, is uninhabited and lacks geodetic or geophysical instruments for real-time monitoring of volcanic or seismic activity. Consequently, the understanding of eruption-related deformation and lava flow evolution relies almost entirely on satellite-based remote sensing (Xu et al., 2023). Limited access, challenging topography, and the dispersed nature of eruptive centres often create data gaps, constraining the ability to track and interpret critical pre-, co-, and post-eruptive changes (Furtney et al., 2018).

Satellite-based remote sensing—especially Synthetic Aperture Radar (SAR)—addresses these challenges by providing frequent, wide-area, and weather-independent coverage of volcanic deformation. Within SAR-based methods, the Small Baseline Subset (SBAS) time-series interferometric technique is particularly effective in high-relief volcanic terrains. SBAS mitigates common issues such as temporal and geometric decorrelation and atmospheric noise, making it well-suited for monitoring deformation in dynamic, uninhabited volcanic regions (Tomar et al., 2018).

2. Study Area and Dataset Used

2.1 Study Area

Wolf Volcano, situated on the northern end of Isabela Island in the Galápagos Archipelago as shown in *Figure 1* is the highest peak in the archipelago, reaching an elevation of 1,710 m (5,610 ft.). It is a classic shield volcano characterized by its distinctive

upturned "soup bowl" morphology, a result of successive low-viscosity basaltic lava flows. Wolf is one of six coalescing volcanoes that form Isabela Island, alongside Ecuador, Darwin, Alcedo, Sierra Negra, and Cerro Azul. Its equatorial location gives it a unique geotectonic context within the Galápagos volcanic system.

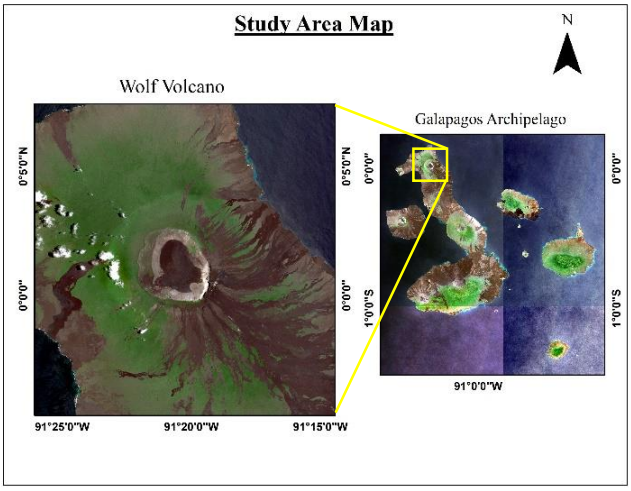

Figure 1: Study Area Map; The Wolf Volcano of the Galapagos Archipelago shown in true colour composite using the Sentinel 2 images

The volcano was named in honour of Theodor Wolf, a 19th-century German geologist who made significant contributions to the scientific study of the Galápagos Islands. It also shares its name with Wolf Island, which lies to the north of the archipelago. Geologically, Wolf Volcano is part of the Galápagos hotspot system, where a stationary mantle plume produces volcanic islands as the Nazca Plate migrates to the east-southeast (Gripp et al., 1990) Wolf is relatively young, with an estimated age of less than 0.5 million years, whereas the underlying oceanic crust is approximately 10 million years old.

Wolf's caldera is one of the largest in the archipelago, measuring approximately 6 × 7 km with a depth of ~700 m and is morphologically comparable to the caldera of Cerro Azul. Its flanks are steep, locally reaching gradients of up to 35°, contributing to its inaccessibility. This combination of remote location, rugged topography, and active hotspot volcanism makes Wolf Volcano an ideal natural laboratory for studying volcanic processes and surface deformation in isolated oceanic island environments.

2.2 Data Used

Sentinel 1A SAR Descending Pass Data

The InSAR data was collected from a satellite platform covering the Wolf Volcano region of the Galápagos Archipelago within a larger scene, as illustrated in the provided image in Figure 2. The study area, outlined by the red boundary, lies in the central part of the image and is defined by coordinates ranging from approximately 91.4473°W to 91.2484°W in longitude and 0.0885°S to 0.1005°N in latitude. Notably, the equator passes through this region.

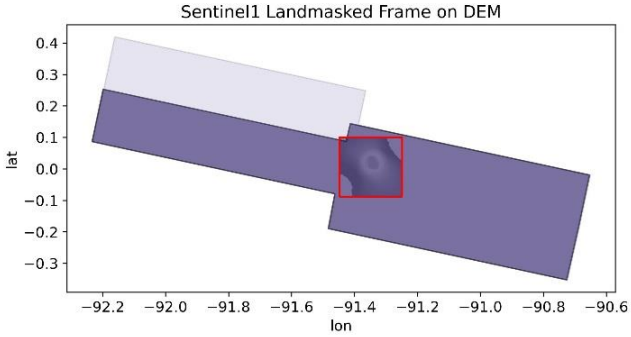

Figure 2: The DEM extracted over the study area

Copernicus DEM 1 arc-second

A Copernicus 1 arc-second Digital Elevation Model covering the Wolf Volcano was used to establish a detailed topographic baseline for the study. The DEM was precisely clipped to match the spatial extent of the InSAR dataset, ensuring consistency in the analysis. This topographic model was essential for correcting terrain-related phase distortions in the InSAR measurements and for examining how surface deformation patterns relate to the volcano's geomorphology and underlying geological structure.

3. Methodology

3.1 Data Acquisition

This study utilized 15 Sentinel-1 burst-mode SAR acquisitions collected in descending orbit between 6 December 2021 and 29 May 2022, covering the 2022 eruption of Wolf Volcano. The datasets were downloaded from the Alaska Satellite Facility (ASF). A Small Baseline Subset (SBAS) time-series InSAR approach was applied to analyse surface deformation patterns using the interferogram pairs as shown below in Table 1.

Table 1: Interferogram pairs made using the Sentinel-1 burst-mode SAR acquisitions collected in descending orbit

Image Pairs		Temporal Baseline	Perpendicular Baseline
Reference	Repeat		
6-Dec-21	12-Dec-21	43.74	6
6-Dec-21	18-Dec-21	58.3	12
12-Dec-21	18-Dec-21	14.56	6
12-Dec-21	24-Dec-21	30.86	12
18-Dec-21	24-Dec-21	16.3	6
18-Dec-21	5-Jan-22	2.63	18
18-Dec-21	17-Jan-22	29.51	30
24-Dec-21	5-Jan-22	13.67	12
5-Jan-22	17-Jan-22	26.88	12
5-Jan-22	29-Jan-22	45.12	24
17-Jan-22	29-Jan-22	18.24	12
29-Jan-22	6-Mar-22	52.71	36
6-Mar-22	18-Mar-22	2.75	12
6-Mar-22	30-Mar-22	50	24
18-Mar-22	30-Mar-22	47.25	12

18-Mar-22	11-Apr-22	67.27	24
30-Mar-22	11-Apr-22	20.02	12
11-Apr-22	23-Apr-22	89.66	12
11-Apr-22	5-May-22	128.59	24
23-Apr-22	5-May-22	218.25	12
23-Apr-22	29-May-22	2.89	36
5-May-22	17-May-22	28.77	12
5-May-22	29-May-22	215.39	24
17-May-22	29-May-22	186.62	12

All processing was performed in Python using the PyGMTSAR library within Google Collab. PyGMTSAR is an open-source Python implementation of the GMTSAR framework, designed for Sentinel-1 interferometry. While GMTSAR is written in C and requires GMT and NETCDF support, PyGMTSAR brings similar functionalities to Python, providing an accessible cloud-based processing environment. The Google Collab workflow included installation of all required Python modules, including plotting libraries, and configuration of a virtual frame buffer for handling graphical outputs. Copernicus 1-arcsecond global DEM tiles and land-mask data covering the study area were also downloaded and integrated into the processing directory to support topographic correction and masking.

3.2 Data Pre-Processing and SBAS Workflow

The Sentinel-1 bursts were first co-registered to ensure precise geometric alignment. Individual bursts were merged to form continuous, gap-free frames. Geocoding was then applied to convert radar coordinates to geographic coordinates and compute the satellite look vector, followed by inverse radar transformation. The workflow is shown below in Figure 4 that has been implemented using the PyGMTSAR in google collab.

SBAS interferometric pairs were generated using a maximum temporal baseline of 36 days and a perpendicular baseline of 215.39 m, ensuring high coherence and minimizing decorrelation (Wu et al., 2024) as shown below in Figure 3. Intensity images were produced by multi-looking the squared amplitude data and applying Gaussian filtering. Phase difference images were computed for each pair, corrected for topography using the DEM, and further multi-looked and Gaussian-filtered to reduce noise.

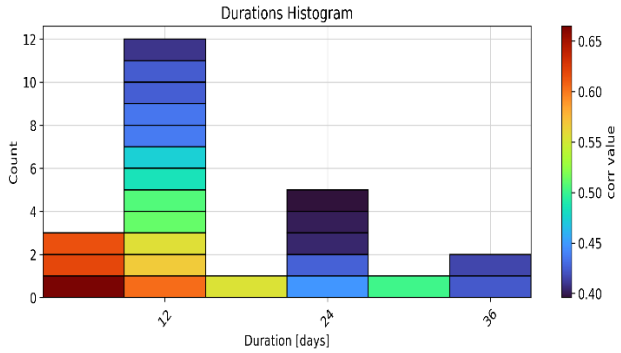

Figure 3: Distribution of InSAR interferogram temporal baselines and associated coherence within the SBAS network.

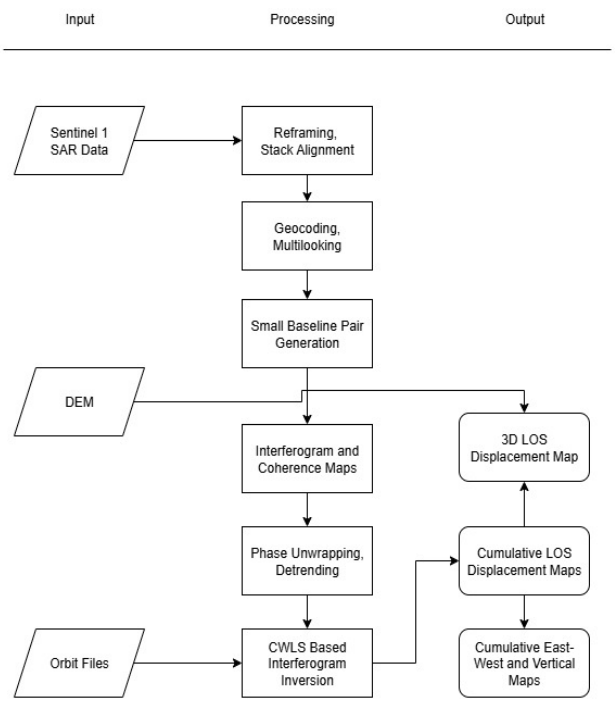

Figure 4: Methodology of SBAS processing in Google Collab using PyGMTSAR

Coherence maps were then derived from the phase and intensity values, providing a measure of interferometric reliability. Goldstein filtering with a 32-pixel patch size was applied to the phase differences to enhance signal quality (Tong & Schmidt, 2016). Interferograms were then unwrapped using the Statistical-cost Network-flow Algorithm for Phase Unwrapping (SNAPHU), which applies a minimum-cost flow optimization and segments the interferogram into reliable tiles before merging them into a single unwrapped phase (C. W. Chen & Zebker, 2002). Only pixels with coherence ≥0.075 were considered for unwrapping to reduce errors in low-coherence areas. The unwrapped interferograms were de-trended, and SBAS time-series displacement maps were generated using a Coherence-Weighted Least Squares (CWLS) approach, where coherence values were used as weights to improve deformation estimates (Tong & Schmidt, 2016).

3.3 Line-of-Sight Displacement and Decomposition

The final SBAS output consisted of Line-of-Sight (LOS) displacement maps. Due to the decommissioning of Sentinel-1B in early 2022, only descending-pass data were available, preventing a full three-dimensional decomposition. Instead, vertical and east-west displacement components were estimated using the descending LOS data, the sensor's incidence angle, and geometric assumptions. Detailed decomposition steps are as follows:-

InSAR (Interferometric Synthetic Aperture Radar) measures deformation along the radar's Line-of-Sight (LOS), and not in standard geographic directions like East, North, or Vertical directions. To interpret this deformation meaningfully, we need to decompose the LOS into those components (Wright, T.J., et al., 2004).

The general LOS displacement is modeled as a projection of the ground displacement vector onto the LOS direction as shown in equation (1):

$$LOS = -(E \cdot \sin\theta \cdot \sin\phi + \mathrm{N} \cdot \sin\theta \cdot \cos\phi + U \cdot \cos\theta), \quad (1)$$

where LOS is the Line of Sight displacement.
E, N, & U are East-West and Upward displacement vectors.
θ = incidence angle
ϕ = azimuth angle

Usually, the North component (N) is considered negligible or poorly resolved by InSAR, so many analyses focus only on decomposing E and U.

3.3.1 LOS Decomposition with both Ascending and Descending Passes

With both passes, we obtain two LOS measurements with differing viewing geometries. Assuming the north component is negligible (N ≈ 0), the equation (1) changes into the following equation (2) as shown below:

$$LOS_i = -(E \cdot \sin\theta_i \cdot \sin\phi_i + U \cdot \cos\theta_i), \quad (2)$$

where $i = a$ and d
a = ascending pass
d = descending pass

The above equation (2) gives a system of two equations in two unknowns i.e. (E, U), which is then solved as the matrix shown below:

$$\begin{bmatrix} LOS_d \\ LOS_a \end{bmatrix} = -\begin{bmatrix} \sin\theta_d \cdot \sin\phi_d + \cos\theta_d \\ \sin\theta_a \cdot \sin\phi_a + \cos\theta_a \end{bmatrix} \cdot \begin{bmatrix} E \\ U \end{bmatrix}$$

Solving this matrix equation (e.g., via least squares) gives E and U values per pixel.

3.3.2 LOS Decomposition Using Only One Pass

When only one viewing geometry is available, the system of equations is underdetermined. So we make simplifying assumptions that are as follows:

It is assumed that whenever there is Vertical motion there is no horizontal motion i.e East-West movement is zero so the equation (1) becomes

$$LOS = -U \cdot \cos\theta$$

Therefore,

$$U = -\frac{LOS}{\cos\theta}, \quad (3)$$

Again for the East-West motion we assume that the Vertical motion is zero, so the equation (1) gets reduced to:

$$LOS = -E \cdot \sin\theta \cdot \sin\phi$$

Therefore,

$$E = -\frac{LOS}{\sin\theta \cdot \sin\phi}, \quad (4)$$

Thus the above equation (3) and (4) are then solved to get displacement in Vertical and East-West directions. These assumptions yield either the vertical or east-west displacement map. Although approximate, this approach is widely used in volcano and subsidence studies when data is limited (Zhang, L., et al., 2021). While full decomposition with two passes is preferred, this one-pass method offers valuable first-order insights in the absence of ascending data.

4. Results and Discussion

The deformation pattern associated with the 2022 eruption of Wolf Volcano were investigated using a combination of Sentinel-1 SBAS-derived displacement maps in Line of Sight and approximate East-West and Vertical directions which provided the insights into the spatio-temporal dynamics of the eruption, capturing surface motion.

The interferogram network as shown below in Figure 5, constructed from descending-pass Sentinel-1 burst data, was processed using the SBAS approach, the coherence maps were then used to weight the interferograms for the time inversion to generate cumulative Line-of-Sight (LOS) displacement maps.

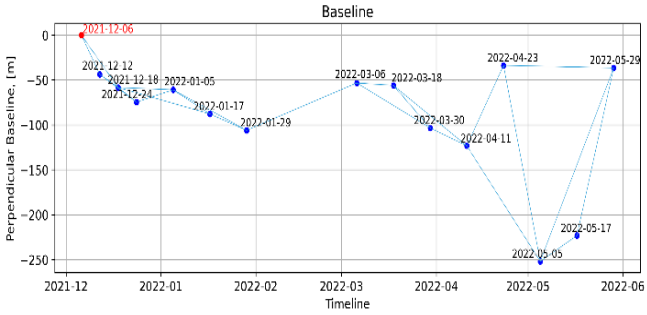

Figure 5: Small Baseline Interferogram network using Sentinel 1 Burst Data

The 3 dimensional line of sight map as shown in Figure 6 reveals a clear deformation pattern across Wolf Volcano. By seeing the 3D LOS displacement map where it is observed significant uplift is observed along the south eastern flank, spatially coinciding with the mapped lava flows, while the central caldera exhibits pronounced subsidence. The latter is interpreted as the result of magma withdrawal from a shallow reservoir beneath the summit, with the asymmetric westward extension of the subsidence zone likely reflecting variations in crustal thickness or structural weaknesses.

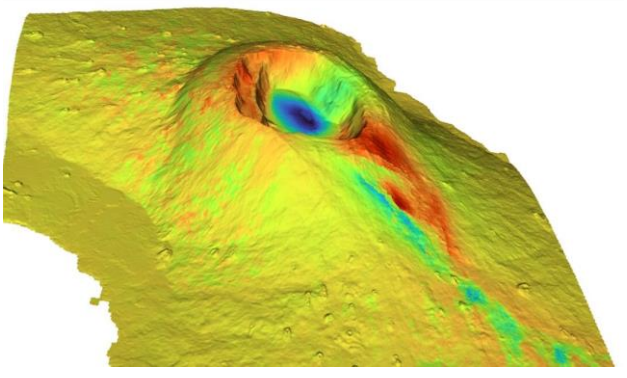

Figure 6: 3 Dimensional Line Of Sight Displacement Map

Vertical displacement estimates, derived from the LOS data using descending-pass decomposition, provide further insight into the temporal evolution of deformation. The Figure 7 shows that prior to the eruption, between 6 December 2021 and 5 January 2022, vertical movement was minimal, indicating a stable pre-eruptive state. Following the eruption onset on 7 January, strong uplift developed in the central volcanic region, reaching approximately +60 mm by late March to early April. In contrast, the southeastern flank experienced subsidence of up to –55 mm, likely linked to magma evacuation or flank instability.

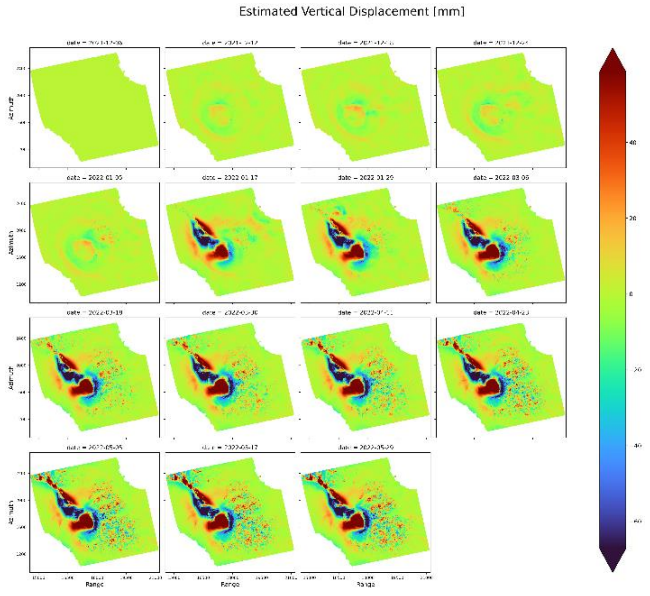

Figure 7: Cumulative approximate Vertical Displacement Maps

After the eruption ended in mid-April, both uplift and subsidence zones stabilised, indicating a transition to post-eruptive equilibrium.

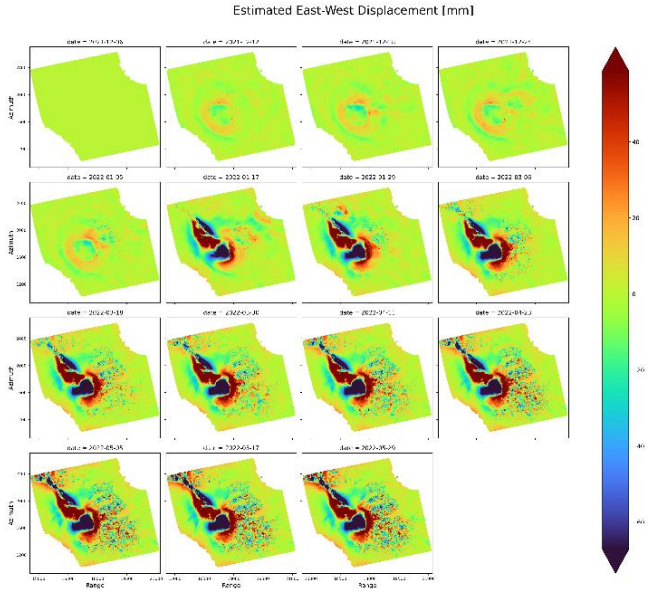

Figure 8: Cumulative approximate East-West Displacement Maps

The above Figure 8 shows the estimated East–west displacement maps that reveal a complementary pattern of lateral movement. No significant horizontal displacement occurred before the eruption. However, from 17 January onwards, the south eastern flank shifted westward by as much as –70 mm, while the north western flank moved eastward by up to +50 mm. This bilateral motion, peaking in late March to early April, is consistent with dyke intrusion or lateral spreading driven by magma forcing the flanks apart. By late May, horizontal movement had ceased, indicating the release of eruptive stresses.

5. Conclusion

This study applied Sentinel-1 InSAR time-series analysis to investigate ground deformation associated with the 2022 eruption of Wolf Volcano, Galápagos. The results, presented in radar coordinates, show that the south eastern flank appearing in the upper-left portion of the displacement maps experienced subsidence, while the summit region exhibited uplift. These deformation patterns evolved from a pre-eruptive phase of minimal movement to rapid inflation during the early eruption, followed by a post-eruptive stabilization.

The spatial arrangement of uplift at the summit and subsidence on the south eastern flank suggests magma pressurization beneath the summit accompanied by lateral magma transport toward the flank. These observations are consistent with eruption reports from the Smithsonian Institution (Venzke, 2024), which note fissure activity on the southern and south eastern flanks during this event.

By capturing the timing, magnitude, and spatial distribution of deformation, InSAR has proven to be a valuable tool not only for volcanic hazard assessment but also for broader geographic research. Its ability to provide precise, spatially continuous measurements over remote and inaccessible regions makes it a powerful method for understanding surface change processes in complex volcanic landscapes such as the Galápagos.

Acknowledgement

The authors gratefully acknowledge the European Space Agency (ESA) for providing the Sentinel-1 SAR products used in this study and the Alaska Satellite Facility (ASF) for facilitating access to the datasets. We extend our thanks to Alexey Pechnikov for developing PyGMTSAR, an open-source, cloud-ready InSAR processing tool that offers an interactive environment with annotations, quality plots, and progress indicators throughout the processing workflow. We also acknowledge the Smithson Institute of Volcanology for providing volcanic eruption data and supplementary information that supported this research. Extending their sincere thanks to the Indian Institute of Remote Sensing (IIRS), ISRO for providing the necessary facilities and support to successfully carrying out this work.

References

Babu, A., & Kumar, S. (2019, June). InSAR coherence and backscatter images based analysis for the Anak Krakatau volcano eruption. In *Proc.*, 87(1). MDPI.

Bayramov, E., Buchroithner, M., Kada, M., & Zhuniskenov, Y. (2021). Quantitative assessment of vertical and horizontal deformations derived by 3D and 2D decompositions of InSAR line-of-sight measurements to supplement industry surveillance programs in the Tengiz Oilfield (Kazakhstan).

Bernard, B., Stock, M. J., Coppola, D., Hidalgo, S., Bagnardi, M., Gibson, S., Gleeson, M. (2019). Chronology and phenomenology of the 1982 and 2015 Wolf volcano eruptions, Galápagos Archipelago. *J. Volcanol. Geotherm. Res.*, 374, 26–38.

Chandni, C. K., Kumar, S., & Babu, A. (2022). SBAS-DInSAR analysis of January 2020 eruption of La Cumbre Volcano, Galapagos Archipelago. *J. Appl. Geophys.*, 206, 104796.

Furtney, M. A., Pritchard, M. E., Biggs, J., Carn, S. A., Ebmeier, S. K., Jay, J. A., … Reath, K. A. (2018). Synthesizing multi-sensor, multi-satellite, multi-decadal datasets for global volcano monitoring. *J. Volcanol. Geotherm. Res.*, 365, 38–56.

Global Volcanism Program (2025). St. Helens (321050) in [Database] *Volcanoes of the World* (v. 5.3.0; 17 Jul 2025). Distributed by Smithsonian Institution, compiled by Venzke, E.

Gripp, A. E., & Gordon, R. G. (1990). Current plate velocities relative to the hotspots incorporating the NUVEL-1 global plate motion model. *Geophys. Res. Lett.*, 17(8), 1109–1112.

Kuraoka, S., Nakashima, Y., Doke, R., & Mannen, K. (2018). Monitoring ground deformation of eruption center by ground-based interferometric synthetic aperture radar (GB-InSAR): A case study during the 2015 phreatic eruption of Hakone volcano. *Earth Planets Space*, 70(1), 181.

Lu, Z. (2007). InSAR imaging of volcanic deformation over cloud-prone areas – Aleutian Islands. *Photogramm. Eng. Remote Sens.*, 73(3), 245–257.

Massonnet, D., & Feigl, K. L. (1998). Radar interferometry and its application to changes in the Earth's surface. *Rev. Geophys.*, 36, 441–500.

Mora, O., Lanari, R., Mallorqui, J. J., Berardino, P., & Sansosti, E. (2002, June). A new algorithm for monitoring localized deformation phenomena based on small baseline differential SAR interferograms. In *IEEE Int. Geosci. Remote Sens. Symp.* (Vol. 2, pp. 1237–1239). IEEE.

Pechnikov, A. (2023). *PyGMTSAR: Sentinel-1 Python InSAR – hnikov, A. (2024). PyGMTSAR (Python InSAR), version 2024.2.8.*

Wu, H. A., Zhang, Y., Kang, Y., Wei, J., Lu, Z., Yan, W., … Liu, N. (2024). SAR interferometry on full scatterers: Mapping ground deformation with ultra-high density from space. Remote Sens. Environ., 302, 113965

Xu, X., et al. (2023). The 2022 eruption of Wolf Volcano, Galápagos: The role of caldera ring-faults during magma transfer from InSAR deformation data. *Geophys. Res. Lett.*, 50, e2023GL103704.